Dalton Transactions

ROYAL SOCIETY OF CHEMISTRY

PAPER

View Article Online
View Journal | View Issue



Cite this: *Dalton Trans.*, 2022, **51**, 4447

# Effect of cysteine thiols on the catalytic and anticancer activity of Ru(II) sulfonyl-ethylenediamine complexes†

Feng Chen, [a,b] Isolda Romero-Canelón, [a,c] Abraha Habtemariam, [a] Ji-Inn Song, [a] Samya Banerjee, [a,d] Guy J. Clarkson, [a] Lijiang Song, [a] Ivan Prokes [a] and Peter J. Sadler *[a]

We have synthesized a series of novel substituted sulfonyl ethylenediamine (en) $Ru^{II}$ arene complexes **1–8** of [($\eta^6$-arene)Ru($R^1$-$SO_2$-EnBz)X], where the arene is benzene, $HO(CH_2)_2O$-phenyl or biphenyl (biph), X = Cl or I, and $R^1$ is phenyl, 4-Me-phenyl, 4-$NO_2$-phenyl or dansyl. The 'piano-stool' structure of complex **3**, [($\eta^6$-biph)Ru(4-Me-phenyl-$SO_2$-EnBz)I], was confirmed by X-ray crystallography. The $pK_a^*$ values of their aqua adducts were determined to be high (9.1 to 9.7). Complexes **1–8** have antiproliferative activity against human A2780 ovarian, and A549 lung cancer cells with $IC_{50}$ values ranging from 4.1 to >50 μM, although, remarkably, complex **7** [($\eta^6$-biph)Ru(phenyl-$SO_2$-EnBz)Cl] was inactive towards A2780 cells, but as potent as the clinical drug cisplatin towards A549 cells. All these complexes also showed catalytic activity in transfer hydrogenation (TH) of $NAD^+$ to NADH with sodium formate as hydride donor, with TOFs in the range of 2.5–9.7 $h^{-1}$. The complexes reacted rapidly with the thiols glutathione (GSH) and *N*-acetyl-L-cysteine (NAC), forming dinuclear bridged complexes [($\eta^6$-biph)$_2$$Ru_2$(GS)$_3$]$^{2-}$ or [($\eta^6$-biph)$_2$$Ru_2$(NAC-H)$_3$]$^{2-}$, with the liberation of the diamine ligand which was detected by LC-MS. In addition, the switching on of fluorescence for complex **8** in aqueous solution confirmed release of the chelated DsEnBz ligand in reactions with these thiols. Reactions with GSH hampered the catalytic TH of $NAD^+$ to NADH due to the decomposition of the complexes. Co-administration to cells of complex **2** [($\eta^6$-biph)Ru(4-Me-phenyl-$SO_2$-EnBz)Cl] with L-buthionine sulfoximine (L-BSO), an inhibitor of GSH synthesis, partially restored the anticancer activity towards A2780 ovarian cancer cells. Complex **2** caused a concentration-dependent G1 phase cell cycle arrest, and induced a significant level of reactive oxygen species (ROS) in A2780 human ovarian cancer cells. The amount of induced ROS decreased with increase in GSH concentration, perhaps due to the formation of the dinuclear Ru-SG complex.

Received 13th November 2021,
Accepted 14th January 2022

DOI: 10.1039/d1dt03856g

rsc.li/dalton



## Introduction

Studies of the antiproliferative activity of organometallic complexes, especially the Ir,[1–3] Os,[4] Rh[5,6] and Ru[7,8] complexes, have been stimulated by the clinical success of platinum anticancer drugs such as cisplatin, carboplatin and oxaliplatin.[9–11] The activity of organometallic half-sandwich complexes can be tuned by the choice of the arene, chelating and monodentate ligands.[12,13] In recent years, the possibility of using synthetic organometallic complexes as catalysts for transfer hydrogenation (TH) reactions in cells has emerged as a potential way of modulating intracellular redox states and inducing cancer cell-killing by a mechanism which can circumvent resistance.[14,15] Noyori-type $Ru^{II}$ complex **JS2** [($\eta^6$-*p*-cym)Ru(TsEn)Cl] exhibits potent catalytic TH activity in the reduction of co-enzyme $NAD^+$ to NADH. Up to a 90% decrease in cancer cell viability was observed in the presence of non-toxic doses of sodium formate (Fig. 1), with the ratio of $NAD^+$/NADH greatly decreasing in cancer cells.[16] The analogue complex [($\eta^6$-*p*-cym)Ru(TsEnBz)Cl] shows enhanced activity in the TH of $NAD^+$ with formate as hydride donor,[17] however, the reaction appeared to be hampered by interaction of the $Ru^{II}$ complex with thiol-containing molecules, including the tripeptide glutathione, γ-L-Glu-L-Cys-Gly (GSH, Fig. 1).[17] We have therefore explored the role of GSH in mediating reactions of these half-sandwich organometallic catalysts in this work.

[a]*Department of Chemistry, University of Warwick, Gibbet Hill Road, Coventry CV4 7AL, UK. E-mail: P.J.Sadler@warwick.ac.uk*
[b]*School of Chemistry and Chemical Engineering, Jiangsu University, Zhenjiang 212013, PR China*
[c]*School of Pharmacy, University of Birmingham, Birmingham B15 2TT, UK*
[d]*Department of Chemistry, Indian Institute of Technology (BHU), Varanasi, UP-221005, India*

†Electronic supplementary information (ESI) available. CCDC 2117792. For ESI and crystallographic data in CIF or other electronic format see DOI: 10.1039/d1dt03856g

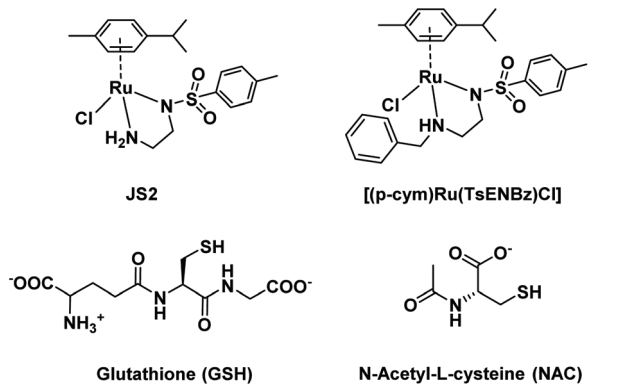


Fig. 1 Structures of Noyori-type $Ru^{II}$ anticancer catalysts, glutathione (GSH) and *N*-acetyl-L-cysteine (NAC).

GSH is an important tripeptide that exists ubiquitously in all eukaryotic cells (in mM concentrations); it can be oxidized, *e.g.* to GSSG, to protect cells from being damaged by reactive oxygen species (ROS, metabolic side products).[18–20] GSH can also interact with metal complexes in cells, and many organometallic complexes are thiophilic.[21] By taking advantage of such interactions, thiols have been used as switch-on probes to trigger luminescence or fluorescence in cells, by either reacting with a probe or by displacement of fluorescent ligands, which can be used to map their distributions in cells.[22,23] We have found that the tethered $Ru^{II}$ complex [Ru($\eta^6$-Ph$(CH_2)_3$-ethylenediamine-N-Ts)Cl] can rapidly react with GSH to form a Ru-SG adduct which can decompose slowly.[24]

In the present work, we have studied the effect of the amino acid cysteine and the tripeptide glutathione on the catalytic and anticancer activity of $Ru^{II}$ sulfonyl ethylenediamine complexes **1–8** [($\eta^6$-arene)Ru($R^1$-$SO_2$-EnBz)X], where the arene is benzene, $HO(CH_2)_2O$-phenyl, or biphenyl, and $R^1$ is various sulfonyl substituents (Table 1). The catalytic TH reduction of $NAD^+$ to NADH using sodium formate as hydride source was studied, as well as reactions of **1–8** with the tripeptide GSH and *N*-acetyl-L-cysteine (NAC) (Fig. 1), and the effect of GSH on the TH of $NAD^+$. The anticancer activity of complexes **1–8** towards A2780 ovarian and A549 lung human cancer cells was determined together with the effect of coadministration with GSH, NAC, and the redox modulator L-buthionine sulfoximine (L-BSO), an inhibitor of GSH biosynthesis. Cell cycle arrest and the influence of GSH on induction of ROS were also investigated. The study revealed an interesting and unusual role for GSH in the biological activity of this class of organometallic transfer hydrogenation catalysts.

Table 1 $Ru^{II}$ complexes studied in this work

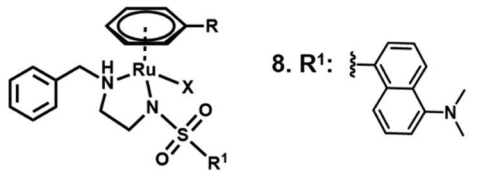


| Complex | R | $R^1$ | X |
|---|---|---|---|
| **1** | H | 4-Me-Ph | Cl |
| **2** | Ph | 4-Me-Ph | Cl |
| **3** | Ph | 4-Me-Ph | I |
| **4** | $O(CH_2)_2OH$ | 4-Me-Ph | Cl |
| **5** | Ph | 4-Nitro-Ph | Cl |
| **6** | Ph | 4-F-Ph | Cl |
| **7** | Ph | Ph | Cl |
| **8** | Ph | Dansyl (Ds) | Cl |

# Results

### Synthesis and characterizations

The chelating diamine ligands [BzEn-$SO_2$-$R^1$], where $R^1$ is phenyl, 4-Me-phenyl, 4-F-phenyl, 4-$NO_2$-phenyl and Dansyl, were synthesized following a reported method,[17] as were complexes **1–8** (Table 1).[25] Triethylamine (4 mol equiv.) and ligand (2–2.1 mol equiv.) were added to the a solution of degassed isopropanol and $Ru^{II}$ dimer [($\eta^6$-arene)$RuCl_2]_2$, and the reactions were then stirred under a $N_2$ atmosphere at 365 K for 10 h. All the synthesized complexes were purified 2× by silica column chromatography (MeOH/DCM, 2 : 8 v/v) and recrystallization, and characterized by NMR spectroscopy ($^1$H, $^{13}$C and $^{19}$F, Fig. S1–S17 in the ESI†), high resolution mass spectrometry (HR-MS, Fig. S18–S25 in the ESI†), and elemental analysis (CHN).

### X-ray crystal structure

A crystal of complex **3** [($\eta^6$-biph)Ru(4-Me-phenyl-$SO_2$-EnBz)I] suitable for X-ray crystallographic analysis was obtained by the slow diffusion of diethyl ether into a saturated methanol solution of complex **3** at ambient temperature. Selected bond lengths and angles for complex **3** are given in Table 2, crystallography data are listed in Tables S1 and S2,† and the molecular structure is shown in Fig. 2. Complex **3** adopts a *pseudo*-tetrahedral geometry with a $\eta^6$-phenyl ring on one face of the metal centre occupying 3 coordination sites. The sulphonamide nitrogen of the ethylenediamine ligand is deprotonated and bound as a monoanionic bidentate ligand to Ru, together with an iodido ligand completing the coordination sphere of the complex.

### $pK_a^*$ determination

The $pK_a^*$ values ($pK_a$ determined in deuterated solvent) of the aqua adducts of complexes **1**, **2** and **4–7** were determined by

Table 2 Selected bond lengths (Å) and angles (°) for complex **3** [($\eta^6$-biph)Ru(4-Me-phenyl-$SO_2$EnBz)I]

| Bonds | Length (Å)/angle (°) |
|---|---|
| Ru–N9 | 2.123(3) |
| Ru–N12 | 2.174(3) |
| Ru–I1 | 2.7434(3) |
| Ru–arene (centroid) | 1.672 |
| N9–Ru–N12 | 78.60(11) |
| N9–Ru–I1 | 90.65(7) |
| N12–Ru–I1 | 83.90(8) |

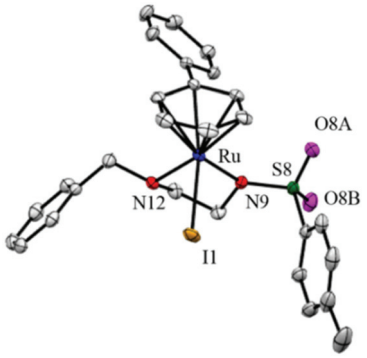


Fig. 2 ORTEP diagram for complex **3** [($\eta^6$-biph)Ru(4-Me-phenyl-$SO_2$EnBz)I]. Ellipsoids are shown at the 50% probability level. All hydrogen atoms have been omitted for clarity.

titration over the pH* range from 2 to 12. The $^1$H NMR chemical shifts of protons of the sulfonyl phenyls as a function pH were fitted to the Henderson–Hasselbalch equation (Fig. S26 in the ESI†). All the p$K_a^*$ values of these aqua complexes are in the range of 9.10–9.75 (Table 3).

### Nucleobase binding

The interaction of complex **2** with model nucleobase 9-ethylguanine (9-EtG) was studied by $^1$H NMR spectroscopy (Fig. S27 in the ESI†). The reactions were performed by titrating a solution of complex **2** (2 mM, 10% MeOD-$d_4$ in $D_2O$) with 9-EtG in $D_2O$ at 310 K, in 0.5 mol equiv. steps. Complex **2** reacted rapidly with 9-EtG, and binding appeared to be complete within 5 min. Adduct formation was confirmed by following a new set of peaks, with slow exchange on the NMR time scale between the aqua adduct of **2** and its 9-EtG adduct. Peaks for complex **2** disappeared when 1.0 mol equiv. of 9-EtG was added, indicating strong binding and completion of the reaction (Fig. S27 in the ESI†).

### Kinetics of transfer hydrogenation

Transfer hydrogenation (TH) of nicotinamide adenine dinucleotide ($NAD^+$) to give NADH was studied in aqueous media using complexes **1–8** as catalysts and sodium formate as hydride source (MeOD-$d_4$/$D_2O$, 1 : 9 (v/v), pH* 7.2 ± 0.1, 310 K). All the kinetic experiments were monitored by $^1$H NMR with $Ru^{II}$, $NAD^+$, and sodium formate in a mol ratio of 1 : 4 : 25. As shown in Table 3, the turnover frequencies (TOFs) for complexes **1–8** are in the range 2.5–9.7 $h^{-1}$, Complex **6** gave the highest TOF (9.7 ± 0.1 $h^{-1}$), while complex **4** gave the lowest (2.5 ± 0.1 $h^{-1}$). Complexes **1** [($\eta^6$-benzene)Ru(4-Me-phenyl-$SO_2$EnBz)Cl] and **2** [($\eta^6$-biph)Ru(4-Me-phenyl-$SO_2$EnBz)Cl] bearing the 4-Me-phenyl-$SO_2$EnBz ligand have similar TOF values (7.5 ± 0.3 and 7.9 ± 0.4 $h^{-1}$, respectively), while complexes **5** and **6** with strong 4-$NO_2$ and 4-F electron-withdrawing groups have higher catalytic efficiency than **2**, with TOF values of 9.1 ± 0.5 and 9.7 ± 0.1 $h^{-1}$, respectively; while complex **7** (phenyl) with the relatively weaker electron-withdrawing group gave a slightly lower TOF value (6.74 ± 0.04 $h^{-1}$).

Table 3 Turnover frequencies for conversion of $NAD^+$ to NADH catalysed by complexes **1–8** and p$K_a^*$ values for the aqua adducts

| Complex | TOF ($h^{-1}$) | p$K_a^*$ |
|---|---|---|
| **1** | 7.5 ± 0.3 | 9.67 ± 0.03 |
| **2** | 7.9 ± 0.4 | 9.3 ± 0.1 |
| **3** | 5.7 ± 1.4 | n. d. |
| **4** | 2.5 ± 0.1 | 9.71 ± 0.05 |
| **5** | 9.1 ± 0.5 | 9.1 ± 0.2 |
| **6** | 9.7 ± 0.1 | 9.12 ± 0.04 |
| **7** | 6.74 ± 0.04 | 9.34 ± 0.07 |
| **8** | 3.7 ± 0.6 | n. d. |

### Reactions with glutathione

Reactions of complex **2** with GSH were investigated *via* a series of concentration-dependent experiments and monitored by $^1$H NMR, at pH* 7.2, (pH* = pH meter reading in deuterated solvent), 310 K. Complex **2** (2 mM) and GSH were mixed in the mol ratio of 1 : *X*, where *X* = 1, 2, 5, 10, respectively, in the mixed solvent of MeOD-$d_4$ and $D_2O$, 1 : 9 (v/v). Reaction of complex **2** with 1.0 mol equiv. GSH led to the disappearance of $^1$H NMR peaks for **2** in the biphenyl ligand region of the spectrum within 10 min, and generated a new set of peaks shifted to lower field (Fig. S28 in the ESI†). No further change in this region was observed with further addition of GSH (2–10 mol equiv.). However, the products were difficult to identify based on the $^1$H NMR spectra alone (Fig. S28 in the ESI†).

### Identification of GSH/NAC adducts by LC-MS

HPLC and LC-MS were used to elucidate the nature of the products from reactions of complex **2** with GSH. Similar reactions with *N*-acetyl-L-cysteine (NAC) were studied for comparison.

Complex **2** (2 mM in MeOH/$H_2O$, 1 : 9 (v/v)) and GSH or NAC (10 mol equiv., in $H_2O$) were mixed in a vial and pre-incubated at 310 K for 24 h (pH 7.10 ± 0.1). As can be seen from Fig. S29,† the reactions proceeded with >95% and 100% conversions to form the $Ru^{II}$-SG and $Ru^{II}$-NAC adducts, respectively, as determined by HPLC. HPLC peak p4, assignable to complex **2**, disappeared after 24 h co-incubation at 310 K, with two new peaks p1 and p2 emerging (Fig. S29 in the ESI†). Subsequently, reactions were studied by LC-MS using the same conditions. MS peaks for dinuclear complexes $[(\eta^6\text{-biph})_2Ru_2(GS)_3]^{2-}$ **2a** and $[(\eta^6\text{-biph})_2Ru_2(NAC\text{-}H)_3]^{2-}$ **2b** are assignable to HPLC peaks p1 and p2, respectively. Displaced free chelating TsEnBz ligand was detected as peak p3. The peak assignments are listed in Table S3 in the ESI.†

Next, the isolation of the dinuclear complexes **2a** and **2b** was attempted by HPLC using a ZORBAX Eclipse XDB-C18 Semi-preparative column (9.4 × 250 mm). Complex **2b** was collected and characterized by $^1$H NMR (Fig. S30 in the ESI†). A high resolution MS peak at 715.6011 *m*/*z* was observed, which corresponds to $[(\eta^6\text{-biph})_2Ru_2(GS)_3+4H]^{2+}$ (**2a** in Fig. S31 in the ESI†), and the high resolution peak at 998.0339 *m*/*z* can be assigned to $[(\eta^6\text{-biph})_2Ru_2(NAC)_3]^+$ (**2b** in Fig. S32 in the ESI†).

### Effect of GSH on transfer hydrogenation of $NAD^+$

Given the high abundance of GSH in mammalian cells, the influence of GSH on the TH of $NAD^+$ catalysed by complex **2** was investigated under similar conditions: **2** (1.4 mM), 10% MeOD-$d_4$/90% $D_2O$ (v/v), with $NAD^+$, GSH and sodium formate ($D_2O$) in the mol ratios of 1 : 4 : *X* : 25, where *X* = 0.2, 0.5, 1 and 2, pH* 7.2, 310 K. $^1H$ NMR spectra were recorded every 5 min. The catalytic efficiency of complex **2** was little affected, with the TOF decreasing slightly from 7.9 ± 0.4 $h^{-1}$ to 6.29 ± 0.53 $h^{-1}$ when 0.2 mol equiv. GSH was present. However, the TOF dropped dramatically to 0.91 ± 0.43 $h^{-1}$ when 0.5 mol equiv. GSH was co-administered. The reaction totally stopped when 1 mol equiv. or more GSH was added, probably due to the completing reaction of **2** with GSH.

### Fluorescence-detected thiol-triggered chelated ligand release from complex 8

The fluorescence of the chelated phenylsulfonyl ethylenediamine dansyl-ligand DsEnBz was fully quenched when it was present as a chelated ligand in complex **8** (Table 1). Complex **8** alone fluoresced only very weakly when dissolved in a mixed solvent of DMSO and $H_2O$ (1 : 9, v/v), Fig. 3. As found above, GSH can react rapidly with complex **8** to form $[(\eta^6\text{-biph})_2Ru_2(GS)_3]^{2-}$, accompanied by the release of the sulfonyl ethylenediamine ligand. Such a reaction should switch-on the fluorescence of DsEnBz through its release from complex **8**. An immediate emission was observed when complex **8** (2 mM in DMSO/$H_2O$, 2 : 8(v/v)) was treated with GSH or NAC (20 mM in $H_2O$, Fig. 3).

The reaction was initially detected by UV-vis spectroscopy at 310 K, pH 7 (Fig. 3a). Next, a *ca.* 200-fold increase in emission intensity was observed on adding GSH (10 mol equiv.) to an aqueous solution of complex **8**, pH 7, 310 K, on excitation at 350 nm (Fig. 3b). NAC induced a stronger increase in fluorescence under the same conditions (*ca.* 1.7-fold stronger than GSH). When excited at 405 nm, the emission intensity was relatively lower, only about 40-fold intensity for GSH and 60-fold for NAC compared to complex **8** alone, Fig. 3c. In order to confirm the importance of the thiol groups in these reactions, complex **8** was reacted with the amino acids L-leucine and L-tryptophan, and the thiol-containing molecule 1-butanethiol. No increase in fluorescence was observed when **8** was mixed with thiol-free amino acids; however, a relatively strong fluorescence emission was found when 1-butanethiol was added, indicating the key role of the thiol group.

### Antiproliferative activity

The antiproliferative activity of complexes **1–8** towards A2780 human ovarian and A549 human lung cancer cells was determined (Table 4). The clinical drug cisplatin (CDDP) was studied as a comparison. As can be seen in Table 4, these complexes gave a broad range of $IC_{50}$ values ranging from 3.57 to >50 μM and 4.1 to 38.5 μM against A2780 human ovarian and A549 human lung cancer cells, respectively. Complex **6** [($\eta^6$-biph)Ru(4-F-phenyl-$SO_2$-EnBz)Cl] was most potent towards A2780 cancer cells ($IC_{50}$, 3.57 ± 0.98 μM), towards which complex **7** [($\eta^6$-biph)Ru(phenyl-$SO_2$-EnBz)Cl] was inactive. However, complex **7** was potent towards A549 lung cancer cells with an $IC_{50}$, 4.1 ± 1.3 μM, comparable to CDDP ($IC_{50}$, 3.1 ± 0.1 μM).

### Effect of L-buthionine sulfoximine on antiproliferative activity

L-Buthionine sulfoximine (L-BSO) is a specific inhibitor of γ-glutamylcysteine synthetase,[26] an enzyme involved in the biosynthesis of GSH. Treatment with L-BSO can scavenge the intracellular GSH levels up to 40%, which effectively hampers

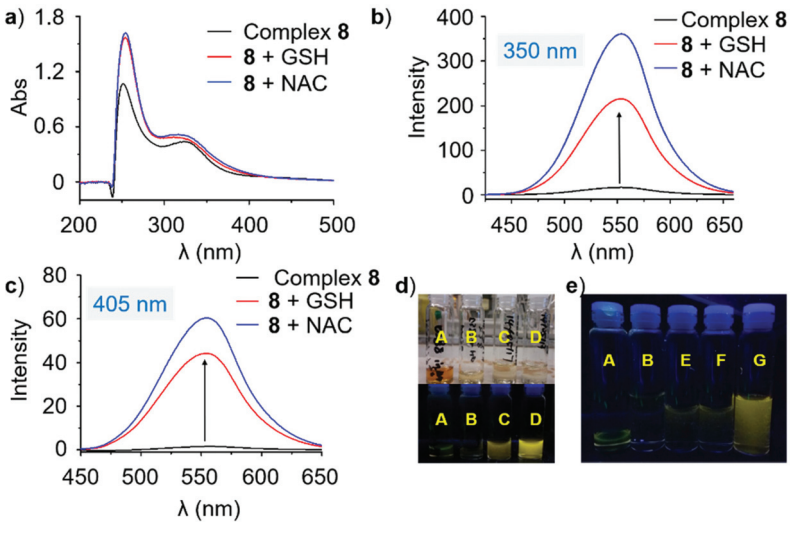


Fig. 3 GSH- and NAC-triggered fluorescence of complex **8**. (a) UV-vis detection of reactions of complex **8** with GSH or NAC; (b) solution excited at 350 nm; (c) solution excited at 405 nm; (d) A: complex **8** in DMSO, B: complex **8** in DMSO/$H_2O$ (1 : 9 (v/v)), C: complex **8** (0.1 mM, DMSO/$H_2O$, 1 : 9 (v/v)) with GSH (2 mM in water) and D: complex **8** (0.1 mM, DMSO/$H_2O$, 1 : 9 (v/v)) with NAC (2 mM in water) under UVA; (e) fluorescence from reactions of complex **8** with L-leucine (E, 10 mol equiv.), L-tryptophan (F, 10 mol equiv.) and 1-butanethiol (G, 10 mol equiv.) under UVA.

Table 4 Anticancer activity of complexes **1–8** towards A2780 human ovarian and A549 human lung cancer cell lines ($IC_{50}$ values, μM)

| | $IC_{50}$ [a] (μM) | |
|---|---|---|
| Complex | A2780 | A549 |
| **1** | 8.32 ± 0.54 | 28.8 ± 2.6 |
| **2** | 11.25 ± 0.08 | 13.5 ± 1.4 |
| **3** | 18.4 ± 1.2 | 32.2 ± 0.7 |
| **4** | 14.25 ± 0.06 | 16.1 ± 2.4 |
| **5** | 3.57 ± 0.98 | 29.8 ± 1.1 |
| **6** | 5.6 ± 0.5 | 13.7 ± 0.1 |
| **7** | >50 | 4.1 ± 1.3 |
| **8** | 39.4 ± 3.4 | 38.5 ± 1.9 |
| **CDDP** | 1.2 ± 0.02 | 3.1 ± 0.1 |

[a] Data are shown as mean ± standard deviation (STD), cell viability was assessed after 24 h incubation with $Ru^{II}$ complexes and washing with PBS.

cellular GSH synthesis.[27] The anticancer activity of complex **2** against A549 human lung cancer cells after co-incubation with L-BSO was determined, to provide insights into the role of GSH in antiproliferative activity. Complex **2** was coadministered with three different concentrations of L-BSO: 1, 5 and 50 μM. After 24 h co-incubation with L-BSO (at concentrations of 1 and 5 μM), the antiproliferative activity of **2** ($IC_{50}$, *ca.* 13 μM) remained unchanged; but increased by 61% to 8.3 ± 0.5 μM when co-treated with 50 μM L-BSO.

### Effect of GSH and NAC on anticancer activity

GSH often acts as a detoxification agent for metal-based drugs in cells, and some drug-resistant cancer cells are capable of generating higher levels of GSH to circumvent damage.[21] *N*-Acetyl-L-cysteine (NAC) is scavenger of reactive oxygen species (ROS), which can block cisplatin related caspase-3 activation and cell apoptosis.[28]

Since complex **2** can react rapidly with GSH to form the dimer **2a** $[(\eta^6\text{-biph})_2Ru_2(GS)_3]^{2-}$, co-administration of complex **2** with GSH (5, 10 and 50 μM) was studied, to investigate the effect of GSH on the antiproliferative activity in A2780 human ovarian carcinoma cells. Cells were incubated with three concentrations of GSH (5, 10 and 50 μM) as controls. The results indicated that GSH exposure only is not toxic towards A2780 cancer cells, Table S4 (in the ESI†). After 72 h of recovery time in drug-free medium, cell survival was evaluated using the sulforhodamine B colorimetric assay. As shown in Fig. 4, the antiproliferative activity decreased gradually with increase of GSH concentration, giving $IC_{50}$ values of 22.41 ± 1.25, 29.9 ± 2.1 and >50 μM towards A2780 cells and, 27.33 ± 0.54, 43.93 ± 3.54 and >50 μM towards A549 cancer cells, for GSH concentrations of 5, 10, and 50 μM, respectively.

Co-treatment with complex **2** and NAC gave rise to a similar trend, in which the anticancer activity decreased with an increase in NAC concentration (under similar conditions as those for GSH above), $IC_{50}$ values are 25.8 ± 0.9, 39.9 ± 0.9 and >50 μM, for NAC concentrations of 5, 10 and 50 μM, respectively.

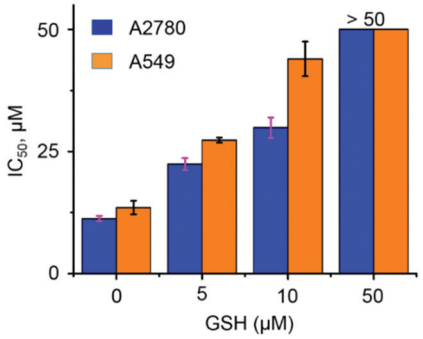


Fig. 4 Effect of co-administration with GSH (5, 10 or 50 μM) on the antiproliferative activity of complex **2** against human A2780 ovarian and A549 lung cancer cells. Data are presented in mean ± standard deviation (STD).

### Cell cycle arrest

A cell cycle analysis for A2780 human ovarian cancer cells treated with the representative complex **2** was performed using propidium iodide staining and flow cytometry. A2780 cancer cells were incubated with $IC_{50}$ or 2 × $IC_{50}$ concentrations of complex **2** for 24 h. In comparison to negative control population, complex **2** increased cell cycle arrest at the G1 phase when the drug concentration increased from $IC_{50}$ to 2 × $IC_{50}$, Fig. 5.

### Reactive oxygen species (ROS)

The level of reactive oxygen species (ROS) induced by complex **2** and GSH in combination with **2** in A2780 human ovarian cancer cells was determined at the $IC_{50}$ concentration of the complex by flow cytometry fluorescence analysis (Fig. 6). These experiments were carried out following previously described protocols.[29] A2780 cancer cells were treated at a fixed $IC_{50}$ concentration of **2** and GSH (0.5 or 5 μM) without any recovery time. The total level of oxidative stress (including $H_2O_2$, peroxy and hydroxyl radicals, peroxynitrite, and NO) in the FITC-A

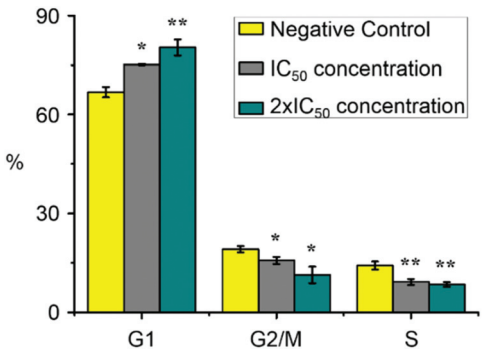


Fig. 5 Cell cycle analysis for A2780 human ovarian cancer cells after 24 h exposure to complex **2** at 310 K at $IC_{50}$ and 2 × $IC_{50}$ concentrations. Cell staining for flow cytometry was carried out using PI/RNase. The percentage of cell populations in each cell cycle phase for the negative control and complex **2** are compared. *p*-Values were calculated after a *t*-test against the negative control data, *$p < 0.05$, **$p < 0.01$.

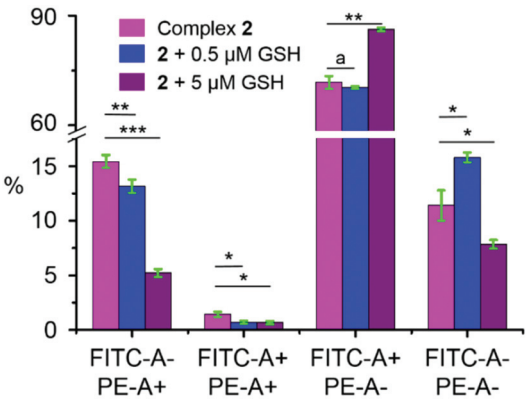


**Fig. 6** ROS induction in A2780 cancer cells exposed to complex **2** alone, **2** with 0.5 μM GSH, and **2** with 5 μM GSH. FITC-A channel detects total oxidative stress, and PE-A channel detects production of superoxide. *p*-Values were calculated after two-tailed Welch's *t*-tests to determine the significance of variations, $^{a}p > 0.05$, $*p < 0.05$, $**p < 0.01$ and $***p < 0.001$.

channel and superoxide production in PE-A channel were monitored. ROS levels were detected in more than 70% of A2780 cancer cells. The populations of A2780 cells showing high fluorescence in FITC-A channel (*ca.* 73.1 ± 1.9%, Table S5 in the ESI†) for complex **2** alone and low fluorescence in channel PE-A (*ca.* 26.8 ± 2.0%), indicate a major induction of oxidative stress in A2780 cancer cells. Interestingly, cell populations in FITC-A-/PE-A+ and FITC-A+/PE-A+ channels decreased with increase of GSH concentration, from *ca.* 16.8 ± 0.8% to *ca.* 5.9 ± 0.5%. However, inversely, cell populations in FITC-A+/PE-A-channels increased when 5 μM GSH was co-administered with **2**, from 71.7 ± 1.7% to 86.3 ± 0.5%, suggesting a higher level of oxidative stress (Table S5 in the ESI†).

## Discussion

The X-ray crystal structure of complex **3** [($\eta^6$-biph)Ru(4-Me-phenyl-$SO_2$-EnBz)I] shows that it has the typical half-sandwich 'piano-stool' geometry (Fig. 2), similar to related $Ru^{II}$ complexes.[25,30] The Ru–N bond lengths of 2.123 Å (Ru–$N^{(-)}$) and 2.174 Å (Ru–N(H)), are close to those reported for [($\eta^6$-*p*-cym)Ru(TsEnEt)Cl] (2.126(9) Å and 2.1702(11) Å, respectively),[25] but the Ru–N12 bond length is 0.08 Å longer than for the related complex [($\eta^6$-biph)Ru(TsEn)Cl] (2.096(4) Å). As expected, the Ru–I bond length is much longer than that of the Ru–Cl bond in [($\eta^6$-biph)Ru(TsEn)Cl] (2.7434(3) Å *versus* 2.4444(11) Å), and close to that in the Os complex [($\eta^6$-*p*-cym)Os(Impy-OH)I]$^+$ (2.7247(4) Å).[26] The N12–Ru–I bond angle of 83.90° is smaller than that of [($\eta^6$-*p*-cym)Ru(EtTsEn)Cl] (87.55°). The remaining bond lengths and angles are similar to those of related $Ru^{II}$ complexes.

In aqueous solution the ability of these halido sulfonyl-ethylenediamine complexes to undergo hydrolysis and generate aqua adducts,[17,25,26] decreases with the halido ligand in the order of Cl ≈ Br > I. Halido complexes with strong δ-donor ligands like en (ethylenediamine) and acac (acetylacetone), hydrolyse quickly and produce basic hydroxido adducts ($pK_a$ > 7), while the π-acceptor ligands like azopyridine, hydrolyse slowly and give more acidic aqua complexes.[26,31] The aqua adducts of the catalysts studied here with high $pK_a^*$ values of 9.1–9.7 (Table 3), would be predominantly protonated in physiological media (pH 7.4). Aqua adducts are usually much more reactive than the corresponding hydroxido adducts and more readily undergo substitution reactions, which is favourable for a catalytic centre.

$Ru^{II}$ sulfonyl ethylenediamine complexes show potent catalytic activity in (sometimes asymmetric) transfer hydrogenation (TH) reactions with ketones, imines, and importantly cellular coenzyme nicotinamide adenine dinucleotide, $NAD^+$.[25,32–36] The efficiency for catalysis of transfer hydrogenation of $NAD^+$ by complex **1** [($\eta^6$-benzene)Ru(TsEnBz)Cl] and **2** [($\eta^6$-biph)Ru(TsEnBz)Cl] was similar (TOFs of 7.5 ± 0.3 $h^{-1}$ and 7.9 ± 0.4 $h^{-1}$, respectively), in comparison to [($\eta^6$-*p*-cym)Ru(TsEnBz)Cl] (7.4 ± 0.1 $h^{-1}$), but decreased with change in arene in the order: biph (**2**) > benzene (**7**) > *p*-cym, which is a slightly different arene order from the previous observations: benzene > biph > *p*-cym.[25] Complex **4** [($\eta^6$-HO$(CH_2)_2$O-phenyl)Ru(TsEnBz)Cl] with hydrophilic side group HO$(CH_2)_2$O- on the phenyl arene has significantly enhanced the water solubility (up to 10 mg $mL^{-1}$ in aqueous solution), while it gave the lowest TOF (2.5 ± 0.1 $h^{-1}$); this may be because the terminal –OH group reversibly triggers rapid tethered ring formation and deformation by binding of the pendant alcohol–oxygen to the metal centre in aqueous solution, thereby hindering $NAD^+$ approach to the Ru centre.[37–39]

Interestingly, Süss-Fink *et al.* have reported a series of dinuclear dithiolato and trithiolato $Ru^{II}$ complexes [($\eta^6$-*p*-cym)$_2$Ru$_2$(SR)$_2$]$^{2+}$ or [$\eta^6$-(*p*-cym)$_2$Ru$_2$(SR)$_3$]$^+$ where R is an aromatic group, which exhibit sub-micromolar anticancer activity against both A2780 and A2780 cisplatin-resistant human ovarian cancer cells.[40–42] Catalytic oxidation of GSH to GSSG by such complexes suggested they can regulate GSH levels in cells.[43] Aldrich-Wright *et al.* have reported the slow degradation of the $Pt^{II}$ complex [(5,6-dimethyl-1,10-phenanthroline)(1*S*,2*S*-diaminocyclohexane)-Pt(II)] by GSH to form the [(5,6-dimethyl-1,10-phenanthroline)$_2$Pt$_2$(SG)$_2$]$^{2+}$, as a GS-bridged dimer.[44] Complex **2** reacted with GSH or NAC to form an Ru-SG/NAC-bridged dimer, that significantly hampered the catalytic TH of $NAD^+$, while retriggering DsEnBz ligand fluorescence of complex **8**, showing that this complex has potential for tracking such ligand dissociation in cells. A recent publication by Briš *et al.* described reactions of organo-ruthenium complexes with cysteine and its analogues studied by mass spectrometry.[45] A ruthenium complex with 1-(4-chlorophenyl)-4,4,4-trifluorobutane-1,3-dione as ligand underwent solvolysis in water to form a [$Ru_2$(*p*-cym)$_2$(OH)$_3$]$^+$ hydroxido-bridged dimer; subsequently hydroxide ligands were displaced by deprotonated cysteine to give the cysteine-bridged dimer similar to complex **2b** in this work.

As an inhibitor of the enzyme γ-glutamyl cysteine synthetase, L-BSO can limit the cellular synthesis of GSH, and enhance ROS levels to induce cell apoptosis. Co-treatment of organometallic $Ru^{II}$ or $Os^{II}$ complexes with L-BSO has been developed as a strategy to overcome GSH mediated detoxification of drugs.[46,47] For example, L-BSO can restore CDDP activity against several CDDP-resistant cancer cell lines. L-BSO has been shown to cause a significant reduction in A2780 cellular GSH levels (*ca.* 50% with 5 μM L-BSO) and a significant enhancement of anticancer activity towards ovarian cancer cells upon co-administration of organo-Os complex [Os($\eta^6$-*p*-cym)(*p*-$NMe_2$-Azpy)I]$PF_6$ with L-BSO (5 μM dose), with 87% improvement in anticancer activity at an equipotent 2 × $IC_{50}$ concentration of the complex.[27,28] However, such restoration of antiproliferative activity by L-BSO only occurs when a complex is already biologically active.[27] In the present work, enhancement of the anticancer activity against A549 cancer cells was observed at an L-BSO concentration of 50 μM with $IC_{50}$ decreasing from *ca.* 13 to 8.3 μM; with levels of GSH reduced to *ca.* 61%.[28] High L-BSO concentrations probably interfere with cellular GSH synthesis, while excessive GSH might react with the complex to destroy catalytic activity but promote the generation of biologically active dinuclear Ru(II) species.[42]

The cell cycle arrest study of complex **2** in A2780 cancer cells revealed a dose-dependent cell population increase in G1 phase (66.7 ± 1.5% to 75.2 ± 0.2% and 80 ± 2% at $IC_{50}$ and 2 × $IC_{50}$ concentrations), but a cell population depletion in G2/M and S phase, which implies that complex **2** is less likely to have DNA as a target site, in agreement with the previous study.[16] DNA-targeted compounds normally cause cell accumulation in the S phase or G2/M phase, *e.g.* cisplatin.[48]

Reactive Oxygen Species (ROS) display important roles in cell metabolism. As respiratory side-products of mitochondria, over-production from ROS damages proteins or causes oxidation of DNA nucleobases to induce cell apoptosis, and ROS-mediated apoptotic signalling is usually associated with reduction of cytosol or mitochondrial GSH levels.[49,50] Organo Ir, Os and Ru complexes have been widely reported as anticancer agents which can induce cell apoptosis *via* ROS-involving pathways.[28,51–53] Complex **2** can induce significant amounts of superoxide in A2780 ovarian cancer cells (up to 16% of the cell population, Table S5 in the ESI†). Co-administration of complex **2** with GSH reduces both superoxide levels and antiproliferative activity against A2780 human ovarian cancer cells. The levels of superoxide showed an inverse relationship with the concentrations of GSH added (Table S5 in the ESI†), and a similar trend in antiproliferative activity with GSH concentration was also observed. This might imply that ROS play an important role in killing cancer cells for these complexes.

## Conclusions

A series of $Ru^{II}$ sulfonyl-substituted ethylenediamine complexes of the type [($\eta^6$-arene)Ru($R^1$-$SO_2$-EnBz)X] (where the arene is benzene, biphenyl or $HOCH_2CH_2O$-phenyl, $R^1$ is 4-Me-phenyl, phenyl, 4-F-phenyl, 4-$NO_2$-phenyl or Dansyl, and X is halide) were synthesized and fully characterized. The half-sandwich structure of complex **3** was confirmed by X-ray crystallography. These complexes retained high potency in transfer hydrogenation of coenzyme $NAD^+$ with formate as hydride donor. The introduction of the substituted arene $HOCH_2CH_2O$-phenyl (complex **4**) significantly improved the water solubility of the complex, albeit with reduced catalytic activity.

Complex **2** [($\eta^6$-biph)Ru(4-Me-phenyl-$SO_2$-EnBz)Cl] bound strongly to 9-ethylguanine to form the **2**-9-EtG-*N7* adduct. However, complex **2** caused only G1 cell cycle arrest in a concentration-dependent manner, and is unlikely to target DNA in cells. Complex **2** exhibited a high affinity for GSH and NAC, to form the Ru-thiolate bridged dimers $[(\eta^6\text{-biph})_2Ru_2(GS)_3]^{2-}$ and $[(\eta^6\text{-biph})_2Ru_2(NAC\text{-}H)_3]^{2-}$. Co-incubation of complex **2** with increasing GSH concentrations effectively reduced induction of reactive oxygen species in cells, and decreased the antiproliferative activity significantly. Such reactions with GSH lead to the release of the chelated diamine ligand, and hence trigger the fluorescence of the free dansyl ligand upon release from complex **8** [($\eta^6$-biph)Ru(DsEnBz)Cl], which might provide a basis for a study of such release in cells. Reactions of $Ru^{II}$ complexes with GSH to form the dinuclear species may offer a new class of TH catalysts that can also form cytotoxic thiolate-bridged complexes in cells. Future work on strategies to control the rate and extent of reactions of these catalysts with GSH, might lead to new concepts in the design of this class of multi-targeting candidate metallodrugs.

## Experimental section

### Materials

Dansyl chloride was purchased from Sigma-Aldrich. The $Ru^{II}$-$\eta^6$-arene precursor dimers were prepared following literature methods,[25,54] as were the ligands (synthesis is presented in ESI†).[17] The solvents used for NMR spectroscopy were purchased from Sigma-Aldrich and Cambridge Isotope Laboratories Inc. Non-dried solvents used in syntheses were obtained from Fisher Scientific. Glutathione and *N*-acetyl-L-cysteine were purchased from Fisher Scientific.

### Synthesis and characterizations

**[($\eta^6$-benzene)Ru(4-Me-phenyl-$SO_2$-EnBz)Cl](1).** All the complexes were prepared according to a reported method:[17] [($\eta^6$-benzene)$RuCl_2$]$_2$ (100 mg, 0.2 mmol) and 4-Me-phenyl-$SO_2$-EnBz (153 mg, 0.45 mmol) were placed in a round-bottom flask, to which 2-propanol (50 mL) and triethylamine (125 μL, 0.9 mmol) were added. The solution was heated under reflux in a nitrogen atmosphere (365 K) overnight with stirring. After this the solvent was removed on a rotary evaporator to give a dark red solid. The crude product was purified by silica column chromatography (MeOH/DCM, 1 : 9 (v/v)), to afford a red solid. Yield = 134.7 mg (65%). **$^1$H NMR** (400 MHz, $CDCl_3$):

$\delta_H$ 2.10–2.24 (m, 2H), 2.33 (s, 3H), 2.40–2.42 (m, 1H), 3.08 (dd, $J$ = 3.1 Hz, 11.2 Hz, 1H), 3.75 (t, $J$ = 10.1 Hz, 1H), 4.19 (q, $J$ = 10.8 Hz, 13.2 Hz, 1H), 4.85 (dd, $J$ = 10.1 Hz, 13.4 Hz, 1H), 5.70 (s, 6H), 7.14 (d, $J$ = 8 Hz, 2H), 7.30–7.32 (m, 2H), 7.35–7.38 (m, 3H), 7.71 (d, $J$ = 8.1 Hz, 2H); **$^{13}$C NMR** (125.73 MHz, $CDCl_3$): $\delta_c$ 21.4, 48.3, 55.5, 62.2, 83.1, 127.3, 128.4, 128.7, 128.9, 129.3, 135.7, 140.1, 140.7; HR-MS: calcd for $[C_{22}H_{25}N_2O_2SRu]^+$ 483.0680 $m/z$, found: 483.0683 $m/z$. Elemental analysis: calcd for $[C_{22}H_{25}N_2O_2SRuCl]0.1(H_2O)$: C, 50.83%; H, 4.89%; N, 5.39%. Found: C, 50.84%; H, 4.81%; N, 5.42%.

**[($\eta^6$-biph)Ru(4-Me-phenyl-SO$_2$-EnBz)Cl] (2).** Complex **2** was obtained following the method described for complex **1**, where $[(\eta^6\text{-biph})RuCl_2]_2$ (100 mg, 0.153 mmol), 4-Me-phenyl-SO$_2$-EnBz (110 mg, 0.32 mmol) and triethylamine (89 μL, 0.64 mmol) were added. The crude product was purified by silica column chromatography (MeOH/DCM, 1 : 9 (v/v)), giving an orange-red solid. Yield = 132.7 mg (73%). **$^1$H NMR** (400 MHz, $CDCl_3$): $\delta_H$ 1.89–1.95 (m, 1H), 2.11–2.17 (m, 2H), 2.34 (s, 3H), 3.08 (dd, $J$ = 3.6 Hz, 11.2 Hz, 1H), 3.59 (q, $J$ = 10.4 Hz, 13.2 Hz, 1H), 3.73 (t, $J$ = 11.5 Hz, 1H), 4.38 (dd, $J$ = 3.9 Hz, 13.3 Hz, 1H), 5.47 (t, $J$ = 7.7 Hz, 1H), 5.98–6.01 (m, 2H), 6.06 (t, $J$ = 5.6 Hz, 1H), 6.57 (d, $J$ = 5.4 Hz, 1H), 7.03–7.05 (m, 2H), 7.15 (d, $J$ = 8.0 Hz, 2H), 7.28–7.31 (m, 4H), 7.53–7.56 (m, 2H), 7.72 (d, $J$ = 8.1 Hz, 2H), 7.80–7.83 (m, 2H); **$^{13}$C NMR** (125.73 MHz, $CDCl_3$): $\delta_C$ 21.4, 48.3, 53.9, 60.5, 78.7, 78.7, 86.4, 88.1, 89.0, 90.4, 127.4, 128.0, 128.2, 128.7, 129.1, 129.4, 129.6, 134.7, 135.7, 140.0, 140.8; HR-MS: calcd for $[C_{28}H_{29}N_2O_2SRu]^+$ 559.0993 $m/z$, found: 559.0990 $m/z$. Elemental analysis: calcd for $[C_{28}H_{29}N_2O_2SRuCl]0.3(H_2O)$: C, 56.09%; H, 4.98%; N, 4.67%. Found: C, 56.02%; H, 5.01%; N, 4.73%.

**[($\eta^6$-biph)Ru(4-Me-phenyl-SO$_2$-EnBz)I] (3).** Complex **3** was obtained following the method described for complex **1**, where $[(\eta^6\text{-biph})RuI_2]_2$ (100 mg, 0.098 mmol), 4-Me-phenyl-SO$_2$-EnBz (70 mg, 0.204 mmol) and triethylamine (58 μL, 0.408 mmol) were added. The crude product was purified by silica column chromatography (MeOH/DCM, 2 : 8 (v/v)). A red solid was obtained. Yield = 72.6 mg (54%). **$^1$H NMR** (400 MHz, $CDCl_3$): $\delta_H$ 1.92–1.98 (m, 1H), 2.07–2.15 (m, 2H), 2.35 (s, 3H), 3.14–3.18 (m, 1H), 3.40 (q, $J$ = 10.9 Hz, 13.2 Hz, 1H), 3.94 (t, $J$ = 11.5 Hz, 1H), 4.32 (dd, $J$ = 4.0 Hz, 13.4 Hz, 1H), 5.40 (t, $J$ = 5.6 Hz, 1H), 5.88 (d, $J$ = 5.8 Hz, 1H), 6.04 (t, $J$ = 5.5 Hz, 1H), 6.34 (t, $J$ = 5.7 Hz, 1H), 6.85 (d, $J$ = 6.1 Hz, 1H), 7.00–7.01 (m, 2H), 7.16 (d, $J$ = 8.2 Hz, 1H), 7.29–7.34 (m, 3H), 7.48–7.54 (m, 3H), 7.70 (d, $J$ = 8.1 Hz, 2H), 7.88–7.91 (m, 2H); **$^{13}$C NMR** (125.73 MHz, $CDCl_3$): $\delta_C$ 21.4, 49.4, 53.5, 60.5, 78.6, 85.8, 87.4, 90.3, 127.7, 127.8, 128.3, 128.6, 128.8, 129.1, 129.5, 129.7, 134.8, 135.7, 139.3, 140.7; HR-MS: calcd for $[C_{28}H_{29}N_2O_2SRu]^+$ 559.0993 $m/z$, found: 559.0994 $m/z$. Elemental analysis: calcd for $[C_{28}H_{29}N_2O_2SRuI]0.2(H_2O)$: C, 48.80%; H, 4.30%; N, 4.06%. Found: C, 48.74%; H, 4.17%; N, 3.96%.

**[($\eta^6$-HOCH$_2$CH$_2$O-phenyl)Ru(4-Me-phenyl-SO$_2$-EnBz)Cl] (4).** Complex **4** was obtained following the method described for complex **1**, where $[(\eta^6\text{-HOCH}_2\text{CH}_2\text{O-Ph})RuCl_2]_2$ (100 mg, 0.161 mmol), 4-Me-phenyl-SO$_2$-EnBz (112 mg, 0.33 mmol) and triethylamine (92 μL, 0.66 mmol) were added. The crude product was purified by silica column chromatography (MeOH/DCM, 1 : 9 (v/v)). A bright red solid was obtained. Yield = 104 mg (56%). **$^1$H NMR** (400 MHz, $CDCl_3$): $\delta_H$ 2.12 (td, $J$ = 2.8 Hz, 11.6 Hz, 1H), 2.22 (dd, $J$ = 4.1 Hz, 11.8 Hz, 1H), 2.34 (s, 3H), 2.48 (d, $J$ = 10.1 Hz, 1H), 3.00 (dd, $J$ = 3.8 Hz, 11.4 Hz, 1H), 3.24 (s, broad, 1H), 3.76 (t, $J$ = 11.3 Hz, 1H), 3.92–3.95 (m, 1H), 4.04–4.08 (m, 1H), 4.17 (q, $J$ = 10.3 Hz, 13.3 Hz, 1H), 4.22–4.32 (m, 2H), 4.77 (dd, $J$ = 4.1 Hz, 13.4 Hz, 1H), 5.04 (t, $J$ = 5.2 Hz, 2H), 5.52 (t, $J$ = 5.6 Hz, 1H), 5.56 (dd, $J$ = 1.0 Hz, 5.9 Hz, 1H), 6.48 (t, $J$ = 5.7 Hz, 1H), 7.15 (d, $J$ = 8.0 Hz, 2H), 7.31 (d, $J$ = 7.5 Hz, 2H), 7.35–7.40 (m, 3H), 7.75 (d, $J$ = 8.2 Hz, 2H); **$^{13}$C NMR** (125.73 MHz, $CDCl_3$): $\delta_C$ 21.4, 47.9, 55.9, 60.8, 61.6, 61.9, 66.5, 68.8, 71.5, 87.1, 90.1, 127.6, 128.4, 128.7, 128.8, 129.3, 134.4, 135.7, 139.9, 140.8; ESI-MS: calcd for $[C_{24}H_{29}N_2O_4SRu]^+$ 543.0891 $m/z$, found: 543.0891 $m/z$. Elemental analysis: calcd for $[C_{24}H_{29}N_2O_4SRuCl]$: C, 49.87%; H, 5.06%; N, 4.85%. Found: C, 50.60%; H, 5.06%; N, 4.60%.

**[($\eta^6$-biph)Ru(4-NO$_2$-phenyl-SO$_2$-EnBz)Cl] (5).** Complex **5** was obtained following the method described for complex **1**, where $[(\eta^6\text{-biph})RuCl_2]_2$ (100 mg, 0.153 mmol), 4-NO$_2$-phenyl-SO$_2$-EnBz (105 mg, 0.32 mmol) and triethylamine (90 μL, 0.64 mmol) were added. The crude product was purified by silica column chromatography (MeOH/DCM, 1 : 9 (v/v)). A dark red solid was obtained. Yield = 90 mg (46%). **$^1$H NMR** (400 MHz, $CDCl_3$): $\delta_H$ 1.96–2.02 (m, 1H), 2.09 (td, $J$ = 3.2 Hz, 12.8 Hz, 1H), 2.24 (d, $J$ = 10.4 Hz, 1H), 3.17 (dd, $J$ = 3.6 Hz, 11.0 Hz, 1H), 3.65–3.70 (m, 2H), 4.41 (q, $J$ = 9.4 Hz, 18.6 Hz, 1H), 5.48 (t, $J$ = 5.7 Hz, 1H), 5.94 (t, $J$ = 5.8 Hz, 1H), 6.04–6.07 (m, 2H), 6.51 (d, $J$ = 5.7 Hz, 1H), 7.04–7.06 (m, 2H), 7.31–7.33 (m, 3H), 7.53–7.55 (m, 3H), 7.79–7.82 (m, 2H), 7.92 (d, $J$ = 8.0 Hz, 2H), 8.15 (d, $J$ = 8.0 Hz, 2H); **$^{13}$C NMR** (125.73 MHz, $CDCl_3$): $\delta_C$ 48.2, 53.9, 60.7, 78.5, 78.9, 86.7, 88.2, 88.8, 90.9, 123.4, 127.9, 128.2, 128.4, 128.8, 129.2, 129.5, 129.9, 134.3, 135.4, 148.7; HR-MS: calcd for $[C_{27}H_{26}N_3O_4SRu]^+$ 590.0688 $m/z$, found: 590.0688 $m/z$. Elemental analysis: calcd for $[C_{27}H_{26}N_3O_4SRuCl]$: C, 51.88%; H, 4.19%; N, 6.72%. Found: C, 51.70%; H, 4.22%; N, 6.69%.

**[($\eta^6$-biph)Ru((4-F-phenyl-SO$_2$-EnBz)Cl] (6).** Complex **6** was obtained following the method described for complex **1**, where $[(\eta^6\text{-biph})RuCl_2]_2$ (100 mg, 0.153 mmol), (4-F-phenyl-SO$_2$)EnBz (98 mg, 0.32 mmol) and triethylamine (89 μL, 0.64 mmol) were added. The crude product was purified by silica column chromatography (MeOH/DCM, 1 : 9 (v/v)). A dark red solid was obtained. Yield = 101 mg (54%). **$^1$H NMR** (400 MHz, $CDCl_3$): $\delta_H$ 1.88–1.98 (m, 1H), 2.10 (dt, $J$ = 3.2 Hz, 12.7 Hz, 1H), 2.17–2.20 (m, 1H), 3.08 (dd, $J$ = 4.1 Hz, 11.6 Hz, 1H), 3.62 (dd, $J$ = 10.3 Hz, 13.0 Hz, 1H), 3.69–3.76 (m, 1H), 4.39 (dd, $J$ = 3.9 Hz, 13.0 Hz, 1H), 5.47 (t, $J$ = 5.7 Hz, 1H), 5.97 (t, $J$ = 5.7 Hz, 1H), 6.01 (d, $J$ = 6.0 Hz, 1H), 6.05 (t, $J$ = 5.7 Hz, 1H), 6.55 (d, $J$ = 5.6 Hz, 1H), 7.00 (t, $J$ = 8.8 Hz, 2H), 7.04–7.06 (m, 2H), 7.30–7.32 (m, 3H), 7.51–7.55 (m, 3H), 7.81–7.84 (m, 4H); **$^{13}$C NMR** (125.73 MHz, $CDCl_3$): $\delta_C$ 48.2, 53.9, 60.6, 78.6, 78.8, 86.5, 88.1, 88.9, 90.6, 114.9, 115.1, 128.0, 128.2, 128.7, 129.2, 129.4, 129.7, 129.7, 129.8, 134.6, 135.6, 163.0, 165.0; **$^{19}$F NMR** (376.4 MHz, $CDCl_3$, spectrum referenced to trifluoro-acetic acid at −76.55 ppm): $\delta_F$ −109.9. HR-MS: calcd for $[C_{27}H_{26}FN_2O_2SRu]^+$ 563.0743 $m/z$, found: 563.0742 $m/z$. Elemental analysis: calcd

 

for $[C_{27}H_{26}FN_2O_2SRuCl]1.4(H_2O)$: C, 52.03%; H, 4.66%; N, 4.49%. Found: C, 52.02%; H, 4.24%; N, 4.78%.

**[($\eta^6$-biph)Ru((phenyl-$SO_2$-EnBz)Cl] (7).** Complex **7** was obtained following the method described for complex **1**, where $[(\eta^6\text{-biph})RuCl_2]_2$ (100 mg, 0.153 mmol), phenyl-$SO_2$-EnBz (90 mg, 0.32 mmol) and triethylamine (89 μL, 0.64 mmol) were added. The crude product was purified by silica column chromatography (MeOH/DCM, 1 : 9 (v/v)). A dark red solid was obtained. Yield = 60.3 mg (34%). **$^1$H NMR** (500 MHz, $CDCl_3$): $\delta_H$ 1.88–1.95 (m, 1H), 2.11–2.18 (m, 2H), 3.11 (dd, $J$ = 5.1 Hz, 9 Hz, 1H), 3.58 (dd, $J$ = 10.4 Hz, 13.4 Hz, 1H), 3.71–3.76 (m, 1H), 4.38 (dd, $J$ = 4.2 Hz, 13.4 Hz, 1H), 5.46 (t, $J$ = 5.7 Hz, 1H), 5.98 (d, $J$ = 6.0 Hz, 1H), 6.01 (d, $J$ = 5.7 Hz, 1H), 6.05 (t, $J$ = 5.7 Hz, 1H), 6.58 (d, $J$ = 5.5 Hz, 1H), 7.03–7.05 (m, 2H), 7.29–7.30 (m, 3H), 7.33–7.40 (m, 4H), 7.52 (d, $J$ = 7.5 Hz, 2H), 7.83 (t, $J$ = 8.5 Hz, 4H); **$^{13}$C NMR** (125.73 MHz, $CDCl_3$): $\delta_C$ 48.3, 53.9, 60.5, 78.7, 78.8, 86.4, 88.1, 88.9, 90.5, 127.3, 128.0, 128.1, 128.2, 128.3, 128.6, 129.1, 129.4, 129.6, 130.5, 134.7, 135.7, 142.9; HR-MS: calcd for $[C_{27}H_{27}N_2O_2SRu]^+$ 545.0837 $m/z$, found: 545.0834 $m/z$. Elemental analysis: calcd for $[C_{27}H_{27}N_2O_2SRuCl]$ $0.4(H_2O)$: C, 55.22%; H, 4.77%; N, 4.77%. Found: C, 55.14%; H, 4.62%; N, 4.86%.

**[($\eta^6$-biph)Ru(DsEnBz)Cl] (8).** Complex **8** was obtained following the method described for complex **1**, where $[(\eta^6\text{-biph})RuCl_2]_2$ (100 mg, 0.153 mmol), DsEnBz (123 mg, 0.32 mmol) and triethylamine (89 μL, 0.64 mmol) were added. The crude product was purified by silica column chromatography (MeOH/DCM, 1 : 9 (v/v)). A dark red solid was obtained. Yield = 138 mg (67%). **$^1$H NMR** (400 MHz, $CDCl_3$): $\delta_H$ 1.87–1.97 (m, 1H), 2.09–2.12 (m, 1H), 2.35 (dt, $J$ = 2.7 Hz, 12.7 Hz, 1H), 2.84 (s, 6H), 3.10 (dd, $J$ = 3.9 Hz, 12.7 Hz, 1H), 3.55 (dd, $J$ = 10.5 Hz, 13.2 Hz, 1H), 3.92 (s, broad, 1H), 4.38 (dd, $J$ = 4.0 Hz, 13.5 Hz, 1H), 5.63 (t, $J$ = 5.6 Hz, 1H), 5.99–6.03 (m, 2H), 6.08 (t, $J$ = 5.6 Hz, 1H), 6.52 (d, $J$ = 5.4 Hz, 1H), 7.04–7.06 (m, 2H), 7.12 (d, $J$ = 7.4 Hz, 1H), 7.29–7.32 (m, 3H), 7.39 (t, $J$ = 7.8 Hz, 1H), 7.47–7.53 (m, 4H), 7.83–7.84 (m, 2H), 8.38 (dd, $J$ = 8.6 Hz, 11.7 Hz, 2H), 8.73 (d, $J$ = 8.6 Hz, 1H); **$^{13}$C NMR** (125.73 MHz, $CDCl_3$): $\delta_C$ 45.5, 48.5, 54.36, 60.1, 79.7, 80.2, 85.5, 85.7, 86.5, 92.2, 114.6, 121.5, 123.5, 127.0, 127.1, 127.4, 127.8, 127.9, 128.1, 128.2, 128.3, 128.5, 128.8, 128.9, 129.4, 129.7, 130.0, 130.1, 130.6, 134.7, 135.9, 151.0; HR-MS: calcd for $[C_{33}H_{34}N_3O_2SRu]^+$ 638.1415 $m/z$, found: 638.1419 $m/z$. Elemental analysis: calcd for $[C_{33}H_{34}N_3O_2SRuCl]0.9(H_2O)$: C, 57.49%; H, 5.23%; N, 6.09%. Found: C, 57.41%; H, 4.97%; N, 6.21%.

### X-ray crystallography

Diffraction data for complex **3** were collected on an Oxford Diffraction Gemini four-circle system with an AtlasS2 CCD area detector. The structure of complex **3** was refined by full-matrix least-squares against $F^2$ using Olex2[55] and was solved by with the ShelXT[56] structure solution program using Intrinsic Phasing and refined with the ShelXL[57] refinement package using Least Squares minimisation. The atoms from the sulphonamide nitrogen to the end of the chain (C10 C11 N12 C13) were modelled as disordered over two positions related by a small ruffle in the chain. The occupancy of the two positions was linked to a free variable which refined to 86 : 14. The minor component was refined isotopically. The NH of the major component was located in a difference map though both it and the NH of the minor position were placed at calculated positions for the rest of the refinement. The data were processed by the modelling program Mercury 3.8. X-ray crystallographic data for complex **3** have been deposited in the Cambridge Crystallographic Data Centre under the accession number CCDC 2117792.†

### *In vitro* growth inhibition assays

The antiproliferative activity of complexes **1–8** was determined against A2780 human ovarian and A549 human lung cancer cells. Briefly, 5000 cells per well were seeded in 96-well plates. The plates were left to pre-incubate with drug-free medium at 310 K for 48 h before adding different concentrations of the tested compounds. Exact drug (Ru) concentrations were determined by ICP-OES. A drug exposure period of 24 h was allowed. After this, supernatants were removed by suction and each well was washed with PBS. A further 72 h were allowed for the cells to recover in drug-free medium at 310 K. The Sulforhodamine B (SRB) assay was used to determine cell viability. $IC_{50}$ values, as the concentration that causes 50% cell death, were determined as duplicates of triplicates in two independent sets of experiments and their standard deviations were calculated.

For cell growth inhibition by GSH/NAC with complex **2**, GSH/NAC at concentrations of 5, 10 and 50 μM were added to the cells first, followed by complex **2** (within 10 min), and the cytotoxicity was monitored using the SRB assay described above. After 24 h co-incubation with complex **2** and GSH, cancer cell viability was assessed after washing the cells with PBS.

### Cell cycle arrest

Approximately 1.5 × $10^6$ per well of A2780 human ovarian cancer cells were cultured in a six-well plate and pre-incubated in drug-free media at 310 K for 24 h, after which complex **2** at equipotent $IC_{50}$ concentration were added. After drug exposure for 24 h, supernatants were removed by suction and cells were washed with PBS. Then A2780 cells were harvested using trypsin-EDTA and fixed with cold 70% ethanol for 2 h. DNA staining was obtained by re-suspension of cell pellets in PBS (containing propidium iodide (PI) and RNase). Cell pellets were washed and re-suspended in PBS before being analysed in a Becton Dickinson FACScan flow cytometer using excitation of DNA-bound PI at 536 nm, with emission at 617 nm. Data were processed with Flowjo software.

### ROS determination

ROS/superoxide induction in A2780 cells induced by complex **2** was determined using the Total ROS/Superoxide detection kit (Enzo-Life Sciences) according to the instructions. The analysis was performed *via* Flow cytometry. Generally, 1.0 × $10^6$ of A2780 cells per well were seeded in the six-well plate and then

pre-incubated in drug-free media at 310 K for 24 h (under 5% $CO_2$ humidified conditions), and then drugs were added to triplicates wells at equipotent $IC_{50}$ concentration. After 24 h of drug exposure, supernatants were removed by suction and cells were washed with PBS and harvested. Cell pellets were then re-suspended in PBS buffer containing the orange/green fluorescent reagents to achieve cell staining. Cells were analysed in a BD LSR II flow cytometer (488 nm laser) using FITC-A channel: 575/26 nm for the oxidative stress and PE-A channel: 530/30 nm for superoxide detection. Data were gated using positive-stained (pyocyanin positive control), untreated-stained and untreated-unstained control samples, acquired as instrumental triplicates by using Flowjo V10 for Windows software. All samples were kept under dark conditions to avoid light-induced ROS production.

## Author contributions

F. C., S. B., A. H., and P. J. S. designed the project. F. C. carried out the synthesis and characterisation of ligands and complexes, determined the $pK_a^*$ values, UV-vis spectra and turnover frequencies. I. R.-C. and J.-I. S. carried out the antiproliferative cell studies and related biochemical assays. G. J. C. carried out the X-ray crystallography. L. S. the high resolution mass spectra work, and I. P. the NMR work. All authors contributed to the writing of the paper.

## Conflicts of interest

There are no conflicts to declare.

## Acknowledgements

We thank the EPSRC (grants EP/F034210/1, EP/P030572/1, and EP/M027503/1), China Scholarship Council (CSC; scholarship for F. C.), and Royal Society (Newton-Bhahba International Fellowship, NF151429, for S. B.) for support.

## References

1 Z. Liu and P. J. Sadler, *Acc. Chem. Res.*, 2014, **47**, 1174–1185.
2 W.-Y. Zhang, S. Banerjee, G. M. Hughes, H. E. Bridgewater, J.-I. Song, B. G. Breeze, G. J. Clarkson, J. P. C. Coverdale, C. Sanchez-Cano, F. Ponte, E. Sicilia and P. J. Sadler, *Chem. Sci.*, 2020, **11**, 5466–5480.
3 S. Kuang, X. Liao, X. Zhang, T. W. Rees, R. Guan, K. Xiong, Y. Chen, L. Ji and H. Chao, *Angew. Chem., Int. Ed.*, 2020, **59**, 3315–3321.
4 S. Banerjee and P. J. Sadler, *RSC Chem. Biol.*, 2021, **2**, 12–29.
5 R. M. Lord, M. Zegke, A. M. Basri, C. M. Pask and P. C. McGowan, *Inorg. Chem.*, 2021, **60**, 2076–2086.
6 M. Hanif, J. Arshad, J. W. Astin, Z. Rana, A. Zafar, S. Movassaghi, E. Leung, K. Patel, T. Söhnel, J. Reynisson, V. Sarojini, R. J. Rosengren, S. M. F. Jamieson and C. G. Hartinger, *Angew. Chem., Int. Ed.*, 2020, **59**, 14609–14614.
7 J. M. Cross, T. R. Blower, A. D. H. Kingdon, R. Pal, D. M. Picton and J. W. Walton, *Molecules*, 2020, **25**, 2383.
8 W.-J. Wang, X. Mu, C.-P. Tan, Y.-J. Wang, Y. Zhang, G. Li and Z.-W. Mao, *J. Am. Chem. Soc.*, 2021, **143**, 11370–11381.
9 B. Rosenberg, L. Vancamp, J. E. Trosko and V. H. Mansour, *Nature*, 1969, **222**, 385–386.
10 X. Wang, X. Wang and Z. Guo, *Acc. Chem. Res.*, 2015, **48**, 2622–2631.
11 T. C. Johnstone, K. Suntharalingam and S. J. Lippard, *Chem. Rev.*, 2016, **116**, 3436–3486.
12 S. K. Tripathy, A. C. Taviti, N. Dehury, A. Sahoo, S. Pal, T. K. Beuria and S. Patra, *Dalton Trans.*, 2015, **44**, 5114–5124.
13 X. Wang, X. Wang, S. Jin, N. Muhammad and Z. Guo, *Chem. Rev.*, 2019, **119**, 1138–1192.
14 Y. K. Yan, M. Melchart, A. Habtemariam, A. F. A. Peacock and P. J. Sadler, *J. Biol. Inorg. Chem.*, 2006, **11**, 483–488.
15 Y. Fu, C. Sanchez-Cano, R. Soni, I. Romero-Canelón, J. M. Hearn, Z. Liu, M. Wills and P. J. Sadler, *Dalton Trans.*, 2016, **45**, 8367–8378.
16 J. J. Soldevila-Barreda, I. Romero-Canelón, A. Habtemariam and P. J. Sadler, *Nat. Commun.*, 2015, **6**, 6582.
17 F. Chen, J. J. Soldevila-Barreda, I. Romero-Canelón, J. P. C. Coverdale, J.-I. Song, G. J. Clarkson, J. Kasparkova, A. Habtemariam, V. Brabec, J. A. Wolny, V. Schünemann and P. J. Sadler, *Dalton Trans.*, 2018, **47**, 7178–7189.
18 A. T. Dharmaraja, *J. Med. Chem.*, 2017, **60**, 3221–3240.
19 Y. Kasherman, S. Sturup and D. Gibson, *J. Med. Chem.*, 2009, **52**, 4319–4328.
20 G. Garai-Ibabe, L. Saa and V. Pavlov, *Anal. Chem.*, 2013, **85**, 5542–5546.
21 M. Kartalou and J. M. Essigmann, *Mutat. Res.*, 2001, **478**, 23–43.
22 R. Zhang, X. Yu, Z. Ye, G. Wang, W. Zhang and J. Yuan, *Inorg. Chem.*, 2010, **49**, 7898–7903.
23 T. Zou, C. T. Lum, S. S.-Y. Chui and C.-M. Che, *Angew. Chem., Int. Ed.*, 2013, **52**, 2930–2933.
24 F. Chen, I. Romero-Canelón, J. J. Soldevila-Barreda, J.-I. Song, J. P. C. Coverdale, G. J. Clarkson, J. Kasparkova, A. Habtemariam, M. Wills, V. Brabec and P. J. Sadler, *Organometallics*, 2018, **37**, 1555–1566.
25 J. J. Soldevila-Barreda, P. C. A. Bruijnincx, A. Habtemariam, G. J. Clarkson, R. J. Deeth and P. J. Sadler, *Organometallics*, 2012, **31**, 5958–5967.
26 Y. Fu, M. J. Romero, A. Habtemariam, M. E. Snowden, L. Song, G. J. Clarkson, B. Qamar, A. M. Pizarro, P. R. Unwin and P. J. Sadler, *Chem. Sci.*, 2012, **3**, 2485–2494.
27 I. Romero-Canelón, L. Salassa and P. J. Sadler, *J. Med. Chem.*, 2013, **56**, 1291–1300.

 

28 Y. Fu, A. Habtemariam, A. M. Pizarro, S. H. van Rijt, D. J. Healey, P. A. Cooper, S. D. Shnyder, G. J. Clarkson and P. J. Sadler, *J. Med. Chem.*, 2010, **53**, 8192–8196.
29 I. Romero-Canelón, M. Mos and P. J. Sadler, *J. Med. Chem.*, 2015, **58**, 7874–7880.
30 R. E. Morris, R. E. Aird, P. S. Murdoch, H. Chen, J. Cummings, N. D. Hughes, S. Parsons, A. Parkin, G. Boyd, D. I. Jodrell and P. J. Sadler, *J. Med. Chem.*, 2001, **44**, 3616–3621.
31 E. J. Anthony, E. M. Bolitho, H. E. Bridgewater, O. W. L. Carter, J. M. Donnelly, C. Imberti, E. C. Lant, F. Lermyte, R. J. Needham, M. Palau, P. J. Sadler, H. Shi, F.-X. Wang, W.-Y. Zhang and Z. Zhang, *Chem. Sci.*, 2020, **11**, 12888–12917.
32 S. Hashiguchi, A. Fujii, J. Takehara, T. Ikariya and R. Noyori, *J. Am. Chem. Soc.*, 1995, **117**, 7562–7563.
33 A. Fujii, S. Hashiguchi, N. Uematsu, T. Ikariya and R. Noyori, *J. Am. Chem. Soc.*, 1996, **118**, 2521–2522.
34 K. J. Haack, S. Hashiguchi, A. Fujii, T. Ikariya and R. Noyori, *Angew. Chem., Int. Ed. Engl.*, 1997, **36**, 285–288.
35 X. Li, W. Chen, W. Hems, F. King and J. Xiao, *Org. Lett.*, 2003, **5**, 4559–4561.
36 X. Li, X. Wu, W. Chen, F. E. Hancock, F. King and J. Xiao, *Org. Lett.*, 2004, **6**, 3321–3324.
37 A. M. Pizarro, M. Melchart, A. Habtemariam, L. Salassa, F. P. A. Fabbiani, S. Parsons and P. J. Sadler, *Inorg. Chem.*, 2010, **49**, 3310–3319.
38 F. Martínez-Peña, S. Infante-Tadeo, A. Habtemariam and A. M. Pizarro, *Inorg. Chem.*, 2018, **57**, 5657–5668.
39 S. Infante-Tadeo, V. Rodríguez-Fanjul, A. Habtemariam and A. M. Pizarro, *Chem. Sci.*, 2021, **12**, 9287–9297.
40 A. F. Ibao, M. Gras, B. Therrien, G. Süss-Fink, O. Zava and P. J. Dyson, *Eur. J. Inorg. Chem.*, 2012, 1531–1535.
41 F. Giannini, L. E. H. Paul, J. Furrer, B. Therrien and G. Süss-Fink, *New J. Chem.*, 2013, **37**, 3503–3511.
42 F. Chérioux, B. Therrien and G. Süss-Fink, *Inorg. Chim. Acta*, 2004, **357**, 834–838.
43 F. Giannini, G. Süss-Fink and J. Furrer, *Inorg. Chem.*, 2011, **50**, 10552–10554.
44 S. Kemp, N. J. Wheate, M. J. Pisani and J. R. Aldrich-Wright, *J. Med. Chem.*, 2008, **51**, 2787–2794.
45 A. Briš, J. Jašík, I. Turel and J. Roithová, *Dalton Trans.*, 2019, **48**, 2626–2634.
46 E. Păunescu, M. Soudani, P. Martin, R. Scopelliti, M. L. Bello and P. J. Dyson, *Organometallics*, 2017, **36**, 3313–3321.
47 I. Romero-Canelón and P. J. Sadler, *Inorg. Chem.*, 2013, **52**, 12276–12291.
48 C. M. Sorenson, M. A. Barry and A. Eastman, *J. Natl. Cancer Inst.*, 1990, **82**, 749–755.
49 M. L. Circu and T. Y. Aw, *Free Radicals Biol. Med.*, 2010, **48**, 749–762.
50 M. P. Murphy, *Biochem. J.*, 2009, **417**, 1–13.
51 S. Kuang, X. Liao, X. Zhang, T. W. Rees, R. Guan, K. Xiong, Y. Chen, L. Ji and H. Chao, *Angew. Chem., Int. Ed.*, 2020, **59**, 3315–3321.
52 M. J. Chow, C. Licona, D. Y. Q. Wong, G. Pastorin, C. Gaiddon and W. H. Ang, *J. Med. Chem.*, 2014, **57**, 6043–6059.
53 M. J. Chow, C. Licona, G. Pastorin, G. Mellitzer, W. H. Ang and C. Gaiddon, *Chem. Sci.*, 2016, **7**, 4117–4124.
54 J. Soleimannejad and C. White, *Organometallics*, 2005, **24**, 2538–2541.
55 O. V. Dolomanov, L. J. Bourhis, R. J. Gildea, J. A. K. Howard and H. Puschmann, *J. Appl. Crystallogr.*, 2009, **42**, 339–341.
56 G. M. Sheldrick, *Acta Crystallogr., Sect. A: Found. Adv.*, 2015, **71**, 3–8.
57 G. M. Sheldrick, *Acta Crystallogr., Sect. C: Struct. Chem.*, 2015, **71**, 3–8.